Novel Prostaglandin D Synthase Inhibitors Generated by Fragment-Based Drug Design†

Morten Hohwy,‡,§ Loredana Spadola,‡,|| Britta Lundquist,⊥ Paul Hawtin,# Jan Dahmén,⊥ Ib Groth-Clausen,⊥ Ewa Nilsson,§ Sofia Persdotter,⊥ Karin von Wachenfeldt,⊥ Rutger H. A. Folmer,§ and Karl Edman*,§

Global Structural Chemistry and Global Compound Sciences, AstraZeneca Research and Development, S-43183 Mölndal, Sweden, AstraZeneca Research and Development Lund, S-221 87 Lund, Sweden, and Global Structural Chemistry, AstraZeneca Research and Development, Alderley Park, Mereside, SK104TG, United Kingdom

Received December 4, 2007

We describe the discovery of novel inhibitors of prostaglandin D2 synthase (PGDS) through fragment-based lead generation and structure-based drug design. A library of 2500 low-molecular-weight compounds was screened using 2D nuclear magnetic resonance (NMR), leading to the identification of 24 primary hits. Structure determination of protein–ligand complexes with the hits enabled a hit optimization process, whereby we harvested increasingly more potent inhibitors out of our corporate compound collection. Two iterative cycles were carried out, comprising NMR screening, molecular modeling, X-ray crystallography, and *in vitro* biochemical testing. Six novel high-resolution PGDS complex structures were determined, and 300 hit analogues were tested. This rational drug design procedure culminated in the discovery of 24 compounds with an IC_{50} below 1 μM in the *in vitro* assay. The best inhibitor (IC_{50} = 21 nM) is one of the most potent inhibitors of PGDS to date. As such, it may enable new functional *in vivo* studies of PGDS and the prostaglandin metabolism pathway.

Introduction

High-throughput screening (HTS)[a] is the dominant method for lead generation in the pharmaceutical industry. HTS uses automated miniaturized assays to screen large libraries of typically 10^6 compounds for binders to a given protein target. Although HTS has proven extremely useful, a review from 2004 reports that only about 25% of projects initiated against druggable targets deliver leads.[1] While this can sometimes be attributed to poor assay properties, a more fundamental problem is that no physical compound collection can sufficiently sample chemical space. It is estimated that there exist $\sim 10^{60}$ combinations of molecules with a molecular size of up to 500 Da.[2] Any compound library only covers a minute fraction of this vast chemical space. An additional issue with leads generated through HTS is that they have often been relatively large and hydrophobic.[3] Such compounds are more likely to fail during development than smaller, more hydrophilic compounds.[4] Over the last years, we have therefore seen a trend toward more "leadlike" HTS libraries,[3] with significantly reduced lipophilicity and molecular weight compared to Lipinski's rules.[5]

Fragment-based drug discovery (FBDD) addresses both the sampling problem and physical property issues described above, which in part explains why it grew to become so popular during the first half of this decade.[6–11] FBDD truly represents an alternative hit identification method where low-molecular-weight compounds (typically 150–250 Da, usually referred to as "fragments") are screened for binding to the target protein. Different screening methods exist, such as high-throughput crystallography,[12] nuclear magnetic resonance (NMR),[6,13] mass spectroscopy,[14] or biochemical screening,[15] but all with the same philosophy in mind: to identify small, weakly binding, well-behaving fragments and to use those as starting points for lead generation.

When the search is restricted to fragments with a low level of complexity, a smaller library can be used, because a higher hit rate is expected.[16] In addition, because the chemical space is reduced for fragments (fewer combinations of atoms exist), a more exhaustive exploration can be performed of the possible interactions in the binding pocket. Therefore, a higher binding efficiency (binding energy per heavy atom or pK_d per heavy atom[17]), is usually achieved relative to typical HTS hits.[18]

The identified fragments can subsequently be developed into more potent and drug-like molecules, by either linking them to other, nonoverlapping binders or expanding them and adding extra functionality.[18] At this point, it is essential to have available detailed structural information on the protein−fragment complexes, as generated by X-ray crystallography or NMR experiments.

Prostaglandins are lipid mediators derived from arachidonic acid with diverse physiological roles within the respiratory, cardiovascular, central nervous system (CNS), genitourinary, endocrine, and immune systems. The exact role of each prostaglandin is determined by their cellular context and the receptor expression profile. The various prostaglandins are synthesized from the common precursor PGH_2, which is generated by the cyclooxygenases (COX-1 and COX-2). Prostaglandin D_2 synthase (PGDS) catalyzes the isomerization of PGH_2 to PGD_2. Release of PGD_2 results in a diverse set of responses ranging from sleep promotion[19] and inhibition of platelet aggregation[20] to the attraction of inflammatory cells[21] and bronchoconstriction.[22] Two isoforms of PGDS have been

† Crystallographic coordinates and structure factor amplitudes for all data sets have been deposited in the Protein Data Bank (PDB, accession codes: 1vd0, 2vcw, 2vcz, 2vcx, 2vcq, and 2vd1).

* To whom correspondence should be addressed. Telephone: +46-31-7064991. Fax: +46-31-7763792. E-mail: karl.edman@astrazeneca.com.

‡ These authors contributed equally to this paper.

§ Global Structural Chemistry, AstraZeneca Research and Development Mölndal.

|| Global Compound Sciences, AstraZeneca Research and Development Mölndal.

⊥ AstraZeneca Research and Development Lund.

Global Structural Chemistry, AstraZeneca Research and Development, Alderley Park.

[a] Abbreviations: PGDS, prostaglandin D2 synthase; HTS, high-throughput screening; FBDD, fragment-based drug discovery; COX, cyclooxygenase; GSH, glutathione; NMR, nuclear magnetic resonance; HAC, heavy-atom count, number of heavy atoms.

10.1021/jm701509k CCC: $40.75
Published on Web 03/15/2008

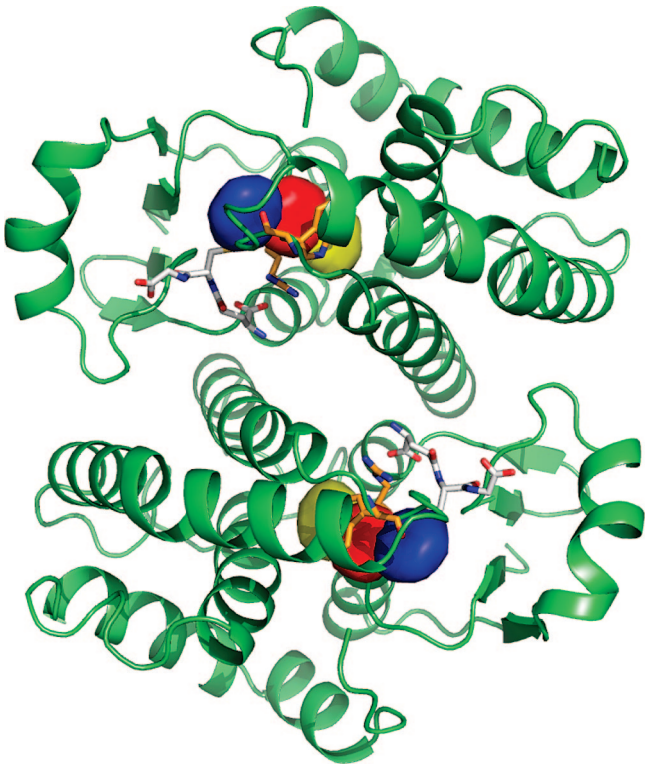

Figure 1. Overview of the human H-PGDS dimer. The yellow sphere represents the inner volume of the substrate-binding site; the red sphere represents the central pocket beneath Trp104; and the blue sphere represents the peripheral, solvent-exposed site. The glutathione cofactor (carbon atoms in white), Arg14, and Trp104 (carbon atoms in gold) are shown in capped sticks to highlight the boundaries of the binding pocket.

isolated, with distinct catalytic properties,[23] tertiary structure,[24] cellular localization, and tissue distribution:[25] the hematopoietic form (H-PGDS), primarily found in white blood cells, and the lipocalin form (L-PGDS), located in the CNS, genital organs, and heart. The difference between the two isoforms is underpinned by the fact that, while H-PGDS requires a glutathione (GSH) cofactor, L-PGDS is independent of GSH for catalysis. The structure of H-PGDS revealed a homodimer with the two active sites along the dimer interface (Figure 1).[26,27] The GSH cofactor was found to bind near the substrate pocket, making extensive contacts to both monomers.

The PGD_2 signal is transmitted by activating the DP1 and the DP2 (CRTH2) receptors. DP1-knockout mice show reduced airway hyper-reactivity, limited eosinophil infiltration, and reduced Th2 cytokine production in an OVA-induced asthmatic model.[28] In addition, polymorphism that impairs the expression of the DP1 gene in humans is associated with a reduced susceptibility to asthma.[29] Interestingly, the DP2 receptor is more related to the chemoattractant receptors than other prostanoid receptors. Indeed, the DP2 receptor has been proven to mediate PGD_2-stimulated chemotaxis of eosinophils and basophils *in vitro*[21] and leukocyte mobilization *in vivo*.[30] A recent study from Uller et al.[31] demonstrated that novel selective DP2 antagonists inhibited the asthmatic response *in vivo*. Mast cell expression of H-PGDS is significantly upregulated during inflammation.[32] Taken together with the fact that PGD_2 is the major lipid mediator released from mast cells upon IgE-mediated allergen challenge,[33–35] H-PGDS is an interesting target for the treatment of asthma and offers the possibility to address both DP1 and DP2 simultaneously. One of the best known PGDS inhibitors is tranilast.[36] While only having modest, micromolar affinity (also for PGES), it is the active anti-inflammatory component of marketed nasal creams and anti-allergy eye drops.

In this work, we apply FBDD to PGDS using a combination of NMR, X-ray crystallography, and modeling. By rationally selecting compounds from our corporate compound collection, we could identify an inhibitor with an IC_{50} of 21 nM with an excellent ligand efficiency of 0.65 kcal mol^{-1} HAC^{-1}.

Results and Discussion

NMR Screening. Fragment-sized compounds have few points for interaction with the target protein, and consequently, the expected affinity for fragments is relatively low, typically in the order of 10–1000 μM. Reliably picking up such weak interactions puts significant demand on the screening method used, in particular, to avoid false positives. We have found NMR screening to be a very robust and versatile method for screening fragments. Dependent upon the specific setup, it is usually possible to observe whether the compounds and/or target proteins are intact and present in the right concentrations during the primary screening. This ensures a minimum of both false positives and false negatives.

NMR-screening methods can be divided in two types: (i) ligand observation methods, such as waterLOGSY,[37] and saturation transfer difference (STD), and (ii) protein observation methods, such as $^{15}N-^{1}H$ heteronuclear single-quantum coherence (HSQC).[6] The latter method offers a higher information content, at the cost of requiring several hundreds of milligrams of ^{15}N-labeled protein. Because PGDS expresses with large yields in *Escherichia coli*, it could easily be isotope-labeled, and we therefore chose the protein-observation method for this work.

The primary NMR screen was conducted on approximately 2500 compounds, divided over two libraries: our general fragment library (2000 molecules) and a targeted library composed of 450 compounds, specifically selected using the structure of the PGDS substrate pocket, as described in the Experimental Section. NMR screening of these two libraries generated 24 primary hits (including 6 from the targeted library), with affinities in the range of $K_d \sim 50$–500 μM. This hit rate of 1% is somewhat low when compared to other reported fragment screens, but this is in part because of the deliberate choice of a comparatively low cutoff (500 μM). Figure 2 illustrates the quality of the NMR data obtained and typical chemical-shift changes that were induced by hit compounds. It is worth noting that we performed the NMR screen without having access to any chemical-shift assignments. Therefore, we do not know what amino acids correspond to the peaks that are indicated by the blue ellipses in this figure. From titrations with reference compounds, however, we knew which the important peaks to be monitored during the analysis of the NMR screen were. Skipping the assignment process has the obvious advantages that we do not have to prepare $^{13}C/^{15}N$-labeled protein, collect the chemical-shift correlation spectra, and analyze them. In particular, for larger proteins (>25 kDa), this can be time-consuming or even impossible to achieve. The disadvantage of not having access to the chemical shifts of all HSQC peaks is that it will be more difficult to probe and explore sites not occupied by the reference compounds. In our PGDS screening data, we found no evidence of such sites; that is, the screened compounds did not induce chemical-shift changes in areas of the spectrum that were unaffected by the reference compounds. The 24 primary hits are shown in Figure 3.

Development of Fragment Hits. The identified fragment hits were subsequently submitted to X-ray crystallography and

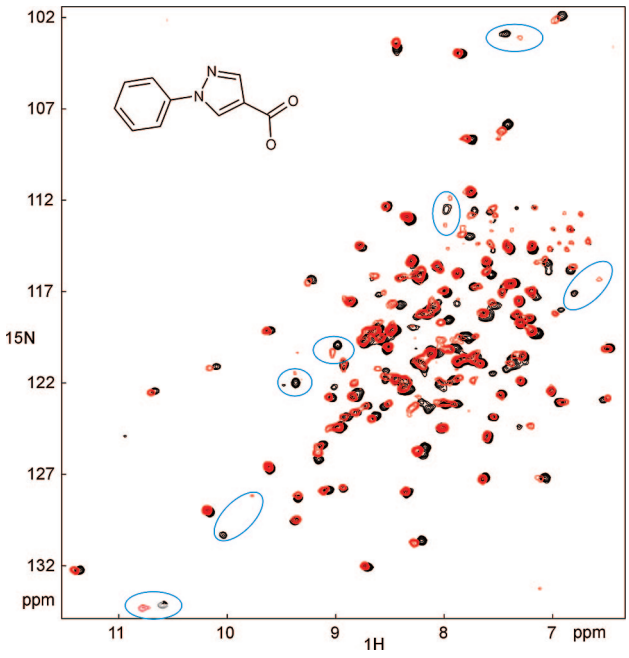

Figure 2. Overlay of two HSQC spectra. The black spectrum is a reference spectrum from the apo protein, i.e., without any compounds present. The red spectrum is that of the mixture that contained the primary hit compound **1**. Peaks whose chemical-shift positions are significantly affected by compound **1** are marked by blue ellipses.

molecular docking. The binding modes determined or hypothesized guided the selection of analogues to these hits from our in-house compound collection. Typically, 10–20 analogues were picked per iteration for each of the hits. These were in turn screened via NMR and/or the *in vitro* assay to identify the best binders within the series of analogues and refine the emerging structure–activity relationship.

Phamacophore Model. The crystal structures of PGDS in complex with tranilast and the primary hit compound **1** (Figure 4) were instrumental for understanding the key interactions involved in complex formation. The benzoyl ring of tranilast overlays very well with the phenyl ring of compound **1** in the inner cavity of the substrate pocket (Figure 4a and 4b), while the position of the amide carbon of tranilast roughly matches that of the N2 in the pyrazole ring (Figure 6a and 6b). The crystal structure of PGDS in complex with compound **1** reveals that this nitrogen accepts a hydrogen bond from a water molecule in the binding site. While this water molecule is conserved in most of the X-ray structures determined subsequently (Figure 4), it is absent in the tranilast complex, where it is displaced by the amide oxygen.

The carboxyl group in tranilast strongly interacts with Arg14, which sits in a central position between the substrate pocket and the GSH molecule. From the early structures, it was evident that there should be alternative ways to create an interaction to this residue. Indeed, looking at the primary NMR hit **2** shown in Figure 6c, we can see that if the quinazoline nitrogen is interacting with the conserved water, the *O*-ethyl group in position 4 would end up in the vicinity of Arg14. This prediction is further encouraged by the fact that the fused phenyl ring also superimposes fairly well with the phenyl rings of compound **1** and tranilast in the inner pocket.

In addition to the interactions outlined above, the molecules are also engaged in a π-stacking interaction with the Trp104 above the second ring; for tranilast, this is accomplished by the conjugated amidic system, which overlays very well with the pyrazole ring of compound **1**. All of these observations are compiled in the phamacophore model outlined schematically in Figure 5.

First Iteration. With this pharmacophore model in hand, the first round of analogues were selected. First, we performed 2D substructural searches in the compound collection using queries derived from the primary hits. The identified compounds were then docked, and the resulting poses filtered on the basis of the ability to form at least two of the interactions described in the pharmacophore model. The final selection was made by visual inspection. The most successful compounds derived from the first iteration around compounds **1** and **2** are shown in Figure 6b and 6c (compounds **5**–**8**). They exhibit up to about 200-fold increase in potency over the primary fragment hits. It is interesting to note that compound **5** is a good binder despite having a hydrogen-bond donor in the 5 position of the pyrazole ring ending up close to the guanidine moiety of Arg14. Therefore, replacing it with a hydrogen-bond acceptor, such as a methoxy or an acidic group, would probably allow for a more favorable interaction, further increasing the potency of the compound. Unfortunately, no such motif was present among the compounds available in house. Molecule **8** has a carbonyl oxygen that, according to docking calculations, overlays quite well with the carbonyl oxygen of tranilast, thus probably displacing the water in a similar manner.

Figure 6d shows compound **3**, whose binding mode is somewhat different from the pharmacophore model described above. If we superimpose this compound onto compound **1**, we see that the five-membered ring and the phenyl ring overlay and that the nitro group is oriented toward the solvent similarly to the carboxy group of compound **1**. It is tempting to assume that the pyrazole ring would be positioned in the phenyl pocket much like the phenyl groups of the other compounds. Surprisingly, however, the X-ray structure revealed that the position of the pyrazole ring is rather shifted compared to the pharmacophoric phenyl ring (Figure 6b). This is due to the presence of yet another water molecule in the binding site that interacts with a N of the pyrazole ring. In addition, a significant shift of the guanidinium moiety of Arg14 can be observed (Figure 4c).

The pyrazole structure of compound **3** prompted us to search for other pyrazole derivatives that fulfilled additional elements of the pharmacophoric criteria (e.g., N interacting with the conserved water and hydrogen-bond acceptor group toward Arg14). This approach also resulted in binders with improved potency, as shown in the results for some of the expanded molecules (molecules **9**–**11**).

Second Iteration. When we started this second iteration, we had enough structural knowledge and confidence about our emerging pharmacophore that we could combine ideas coming from different sources. In particular, parallel to the fragment-based approach, we carried out a separate virtual screening exercise that allowed for the identification of a molecule with micromolar potency (compound **4**, Figure 6e). The docking pose of this compound suggested that it complied with our pharmacophore model, except for the interaction to the conserved water molecule. To follow the shape of the substrate site and avoid a clash with Ile199, the compound orients the central thiazole with a carbon atom in proximity to the conserved water. However, the notable potency of this compound inspired the search for other molecules containing thiazoles as the central ring. Moreover, in this iteration, the 2D substructural search included the possibility of having a pyrazole ring based on compound **3** and the previous expansion. The combination of these ideas was rewarded with compounds of nanomolar potencies (compounds

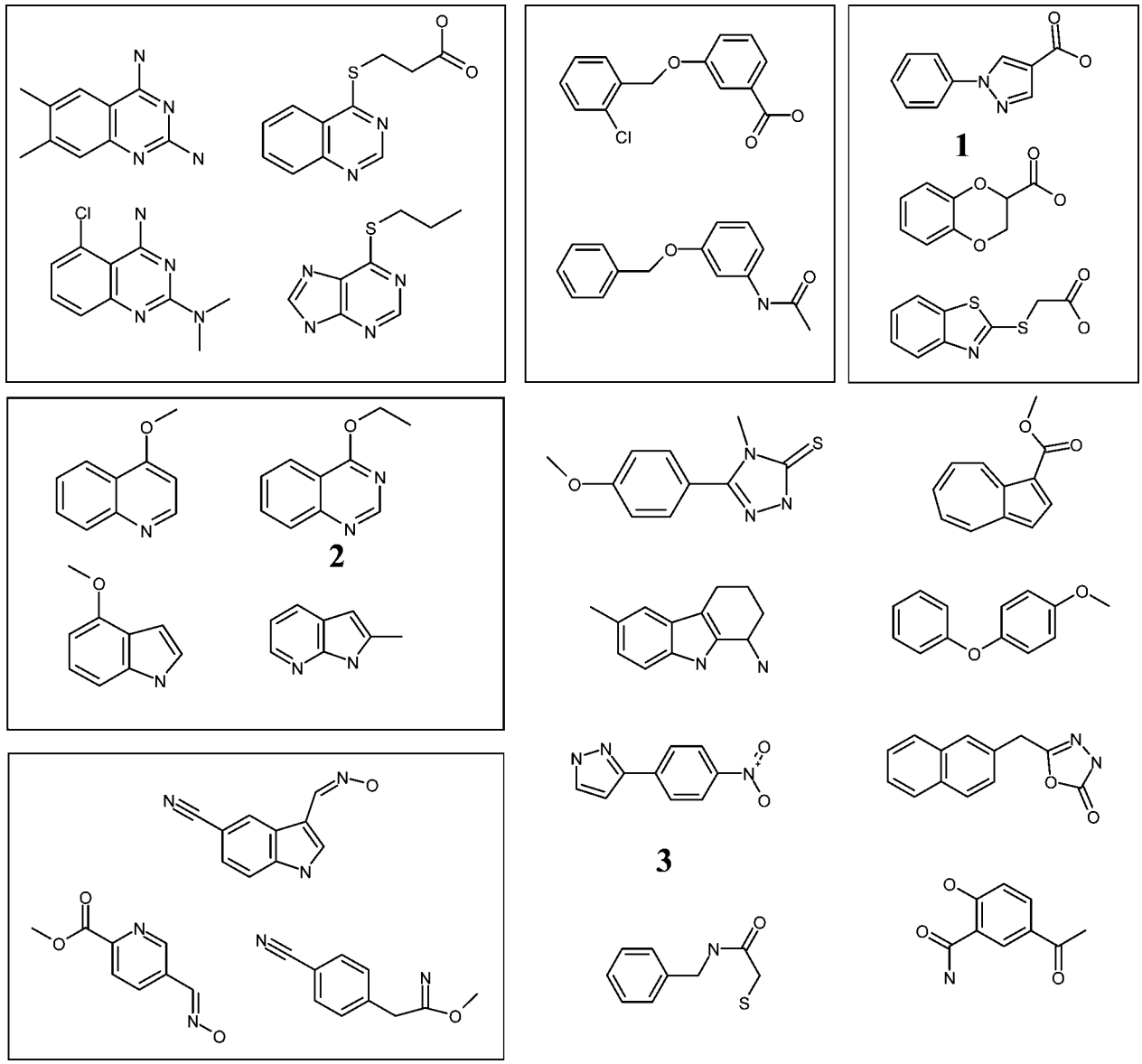

Figure 3. Complete set of primary fragment hits generated by the NMR screen. On the basis of their similarity and hypothesized binding mode, we divided 16 hits into 5 small clusters, while 8 compounds were considered singletons. All of the compounds were acquired from external suppliers.

12–**15**). The cocrystal structure of compound **12** (Figure 4f) confirmed the binding mode hypothesized for compound **4**. Interestingly, the structures from compounds **13** and **14** showed Arg14 in a position similar to that observed when interacting with compound **3**, packing against the central five-membered ring together with the thiazole of the GSH. The importance of the interaction to GSH was confirmed for compound **13**, which exhibited an almost 14 times higher affinity for PGDS in the presence of GSH (Figure 7). The activity of compound **13** on PDGS was further confirmed by its activity in a cellular screening assay, where it was shown to inhibit PMA/Ionomycin-induced PDG2 synthesis in a human mast cell line in the low micromolar range (Figure 8).

Given the high reactivity of the GSH thiole group, we wanted to dismiss the risk of covalent interaction for compounds of exceptional potency. The high-resolution X-ray structures of compounds **13** and **14** rule out any covalent binding. Rather, the high potency is believed to primarily derive from good shape match to the substrate site in combination with the interaction to the conserved water molecule.

The high potency of compound **13** is in good agreement with a recent paper by Hesterkamp et al.,[38] which reports low nanomolar potency for a larger but related compound.

Conclusion

A variety of PGDS inhibitors were identified using fragment-based drug discovery. Iterative expansions around the original hits, employing both X-ray crystallography and computational chemistry, led to the discovery of several novel PGDS inhibitors with nanomolar affinities. In this work, fragment optimization was performed exclusively through iteratively harvesting our corporate compound library for compound analogues, i.e., without the use of synthetic chemistry. Having access to crystallographic information and reliable assay values at all stages of the process allowed for a rational design approach, which rapidly enabled us to progress our midmicromolar fragment hits, improving their affinities by a 100−1000-fold. Moreover, the compounds have good solubility and comparably low molecular weights, resulting in excellent ligand-binding efficiency[39] (Table 1). The solubility follows from working with

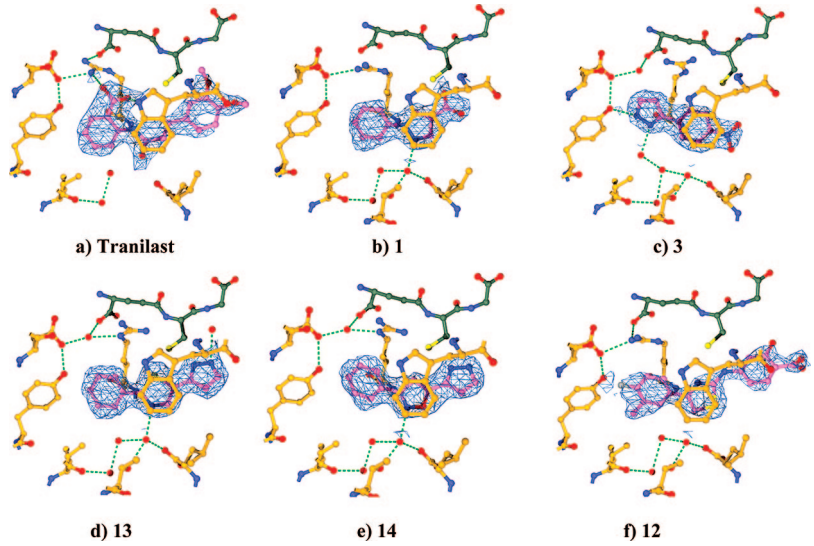

Figure 4. Refined $2mF_o - DF_c$ electron density from the (binding site) structures of PGDS in complex with tranilast (a), the primary hit compound **1** (b), and ligands coming from the expansions: compound **3** (c), compound **13** (d), compound **14** (e), and compound **12** (f). The compounds are shown in purple; the glutathione is shown in olive; and the protein residues are shown in gold. The dashed green lines symbolize putative hydrogen bonds (heteroatoms within 3.2 Å). The structures were solved to resolutions ranging from 1.95 to 2.25 Å.

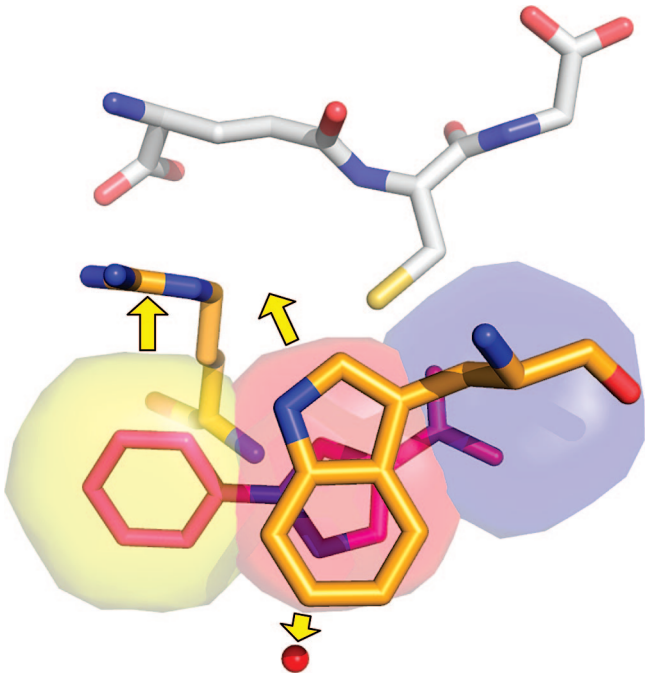

Figure 5. The substrate pocket of PGDS can be subdivided into three different regions based on the placement of the chemical motifs from various inhibitors: the inner cavity (yellow), which is typically occupied by an aromatic ring; the central cavity (red), which is characteristically occupied by a heterocyle; and the peripheral solvent exposed part of the pocket (blue), where the largest structural variation is observed. The potential interactions involved in ligand binding are shown: the yellow arrows indicate hydrogen-bond interactions with Arg14 and a conserved water molecule. Trp104 is involved in a π-stacking interaction with the central heterocycle of the ligand.

a library of highly soluble fragments. The favorable low molecular weight and good binding efficiency underpin the claim that fragments sample chemical space well.[16]

In summary, we carried out two major iterations, obtained the X-ray structures of six complexes, and screened a total of about 300 hit analogues. In this process, we identified several potent inhibitors with the molecular diversity sufficient to evolve into four different lead series (Table 1). Our results show that PGDS is a highly tractable target, and the compounds described should provide a firm platform for further studies of the important prostaglandin metabolism pathways.

Experimental Section

Expression and Purification of the Protein. The protein was expressed in *E. coli* strain BL21(DE3) with an N-terminal 6-His tag. Bacteria were grown in $^1/_2$ LCPA minimal medium in a fermentor at 30 or 37 °C and induced with isopropyl-β-D-thiogalactopyranoside (IPTG) around OD5. To achieve the ^{15}N labeling, ^{15}N-labeled ammonium chloride was present as the sole nitrogen source. A 6 L grow with labeled medium produced 269 cell paste from 6 L of culture at OD28, 13.4 g/L dry weight. Unlabeled protein for crystallization was produced from a 16 L grow, which yielded 454 g paste at OD26, 6.9 g/L dry weight.

Cells were lysed in a buffer consisting of 20 mM Tris at pH 7.5, 300 mM NaCl, 20 mM imidazole, 8.7% glycerol, inhibitor cocktail, and 1 mM β-mercaptoethanol. The lysate was centrifuged at 40000*g* for 30 min. The supernatant was loaded on to a 50 mL Ni-NTA superflow column, which had been equilibrated in 20 mM Tris at pH 7.5, 300 mM NaCl, 20 mM imidazole, and 8.7% glycerol, and the protein was eluted with 20 mM Tris at pH 7.5, 300 mM NaCl, 400 mM imidazole, 8.7% glycerol, and 2 mM β-mercaptoethanol. The eluted protein was concentrated on an S75 column equilibrated in 50 mM Tris at pH 7.5, 50 mM NaCl, 1 mM dithiothreitol (DTT), and 1 mM $MgCl_2$. This two-step purification protocol was sufficient to obtain pure protein, as could be concluded from SDS−PAGE. The final yield was about 75 mg of protein/L of medium.

***In Vitro* Assay.** The PGDS glutathione-*S*-transferase (GST) activity is measured by using MonoChloroBimane (MCB) as a chromogenic substrate. The assay was run at 384-well format, as follows: 60 ng of PGDS was incubated for 15 min at room temperature with 5−250 μM compound (final concentration) in a buffer consisting of 20 mM Tris-HCl at pH 7.2, 0.1% 3-[(3-cholamidopropyl)dimethylammonio]-1-propanesulfonate (CHAPS), 1 mg γ-globulin/mL, and 2 mM $MgCl_2$. γ-Globulin was added to improve stability of the reagents, but also without it, all solutions used are stable for more than 4 h at room temperature. Then, MCB was added to a concentration of 0.15 mM and GSH was added to a concentration of 0.7 mM. After further incubating for 30 min while gently shaking, the reaction was stopped with a mixture of sodium chloroacetate, sodium acetate, and acetic acid at pH 4.3. After another 30 min, the fluorescence was read out (excitation,

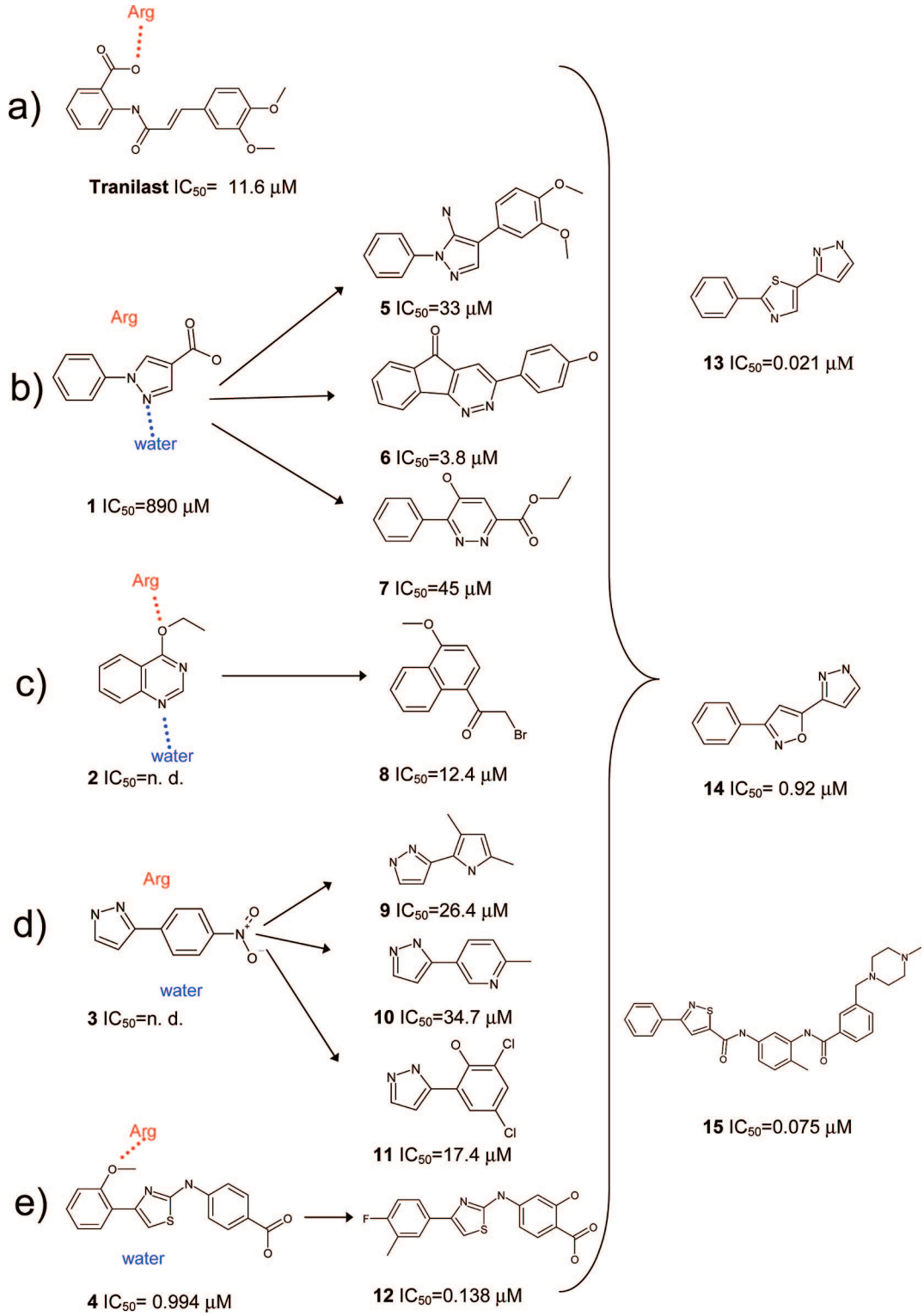

Figure 6. Schematical representation of the expansion process from primary hits (tranilast and compounds **1**–**4**). On the right-hand side are the hits coming from the first expansion (compounds **5**–**12**) and those coming from the second iteration (compounds **13**–**15**). The activity reported is IC_{50} (in micromolars) measured with the GST assay. The arrows show the expanded ligand in relation to their primary counterpart. The curly bracket indicates that the last expansion combined all of the ideas from hits in the previous one. All of the molecules are shown in their putative binding mode with the key arginine and water molecule highlighted for the primary hits. All of the compounds were acquired from external suppliers with the exception of compounds **4** and **15**, which were present in the in-house collection.

390 nm; emission, 478 nm). MCB has a K_m of 0.16 mM and V_{max} of 11 000 FI. Corresponding numbers for GSH are 0.65 mM and 15 000 FI. The assay is linear for 60 min. The signal was approximately 5 times the background, and the Z' factor was 0.8.

Cell-Based *in Vitro* Assay. Compounds with a confirmed inhibitory effect on PDGS were tested in LAD2 cells for inhibition of PDG_2 release. LAD2 is a human mast cell line derived from a bone marrow aspirate from a mast cell sarcoma/leukemia patient.[40] The assay was run in a 96-well format, as follows: cells were seeded at day 0 at a cell density of 7.5×10^5 cells/mL and preincubated overnight. At day 1, cells were preincubated for 30 min at 37 °C with 0.1–30 μM compound (final concentration) before stimulation

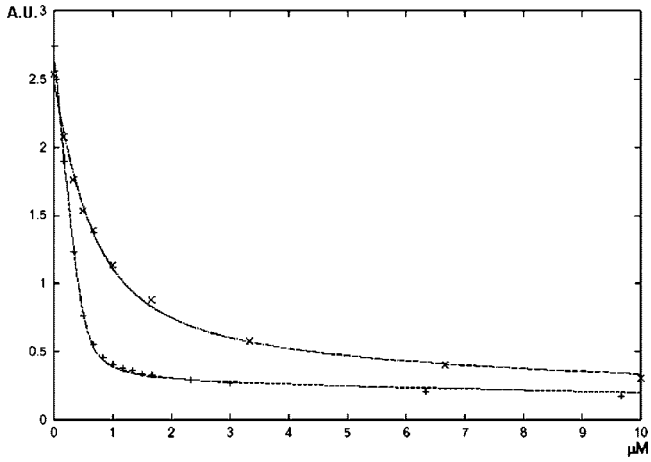

Figure 7. Trp-fluorescent measurements of compound **13** with 2 mM GSH (+) and without GSH (×) present in the buffer, measured as described in the Experimental Section. The resulting dissociation constants were 27 and 374 nM with and wihtout GSH, respectively.

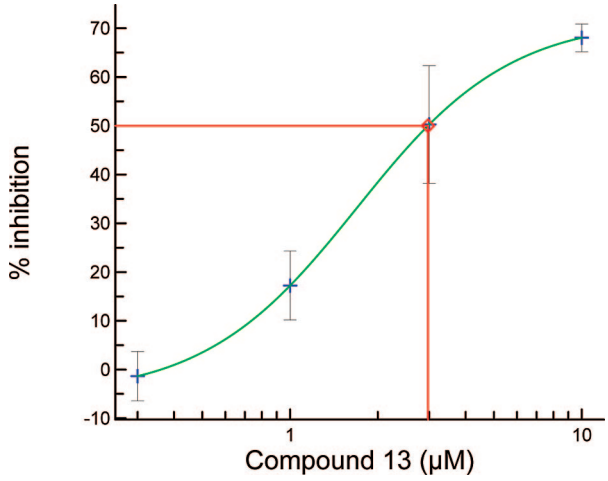

Figure 8. Inhibition of PMA/ionomycin-induced PDG2 in the human mast cell line LAD2 by compound **13**. The figure shows one representative experiment ($n = 3$), where each point represents a mean of duplicate values. Mean EC_{50} for the three experiments was 2.3 ± 0.9 μM, and mean EC_{50} for the experiment illustrated in the graph was 1.7 μM.

with 1 ng/mL PMA and 0.75 μg/mL ionomycin for an additional 30 min. Compounds were dissolved in dimethylsulfoxide (DMSO), resulting in a final DMSO concentration of 0.1%, which was shown to have no effect on the cellular viability and responsiveness. The reaction was stopped by centrifugation at 4 °C and collection of the supernatants. Samples were analyzed using the "prostaglandin D2—MOX express EIA kit" from Cayman Chemical according to the instructions of the manufacturer.

NMR Experiments. NMR samples used for screening contained ~100 μM ^{15}N-labeled protein, in a buffer consisting of 20 mM *N*-2-hydroxyethylpiperazine-*N*′-2-ethanesulfonic acid (HEPES) at pH 7.0 and 20 mM NaCl. There was no GSH present in the original screen. ^{15}N HSQC experiments were recorded at 298 K as TROSY spectra[41] on a Bruker AV600 equipped with a cryoprobe. Typical acquisition time was 60 min per experiment. The compounds were screened in mixtures of 12 at an individual concentration of 400 μM. Prior to each HSQC spectrum, a 4 min waterLOGSY[37] spectrum was recorded on the same sample; if analysis of the HSQC spectrum subsequently would indicate that one of the compounds in the cocktail was a hit, the 1D waterLOGSY spectrum helped identifying that active compound. This allowed for a more efficient deconvolution of the 2D screening data.

Table 1. Representatives from the Four-Hit Series

Structure	IC_{50} (μM)	cLogD[a]	M.W.	L.E.[b] (kcal/mol/HAC)
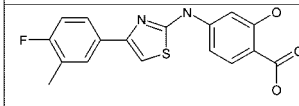	0.138	-0.2	344	0.39
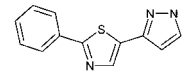	0.021	3.2	227	0.65
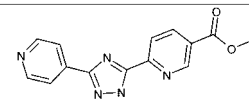	1.5	2.0	281	0.38
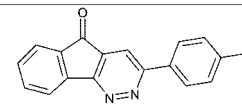	3.8	3.6	272	0.35

[a] ACD log *D* at pH 7.4. For the bottom three compounds, *c* log *P* = *c* log *D*. [b] Ligand-binding efficiency (L.E.) = $-RT$ ln (IC_{50})/HAC, where HAC is the number of heavy atoms.

Compounds were stored as 100 mM DMSO-d_6 stock solutions on 384 well plates. The addition of compounds to the protein buffer introduced 4.8% DMSO-d_6, which was used to lock the spectrometer. A SampleRail system (Bruker) connected to a Tecan Gemini robot was used for automated sample preparation of each sample immediately prior to the execution of NMR experiments. Spectra were processed with NMRpipe[42] and analyzed with NMRview.[43] In total, ~200 2D spectra were recorded for the primary screen, and another 150 spectra were recorded for deconvolution of the hits and K_d determinations. No automation was used for the analysis; we considered a simple overlay of each screening spectrum with the reference to be the most robust and sufficiently quick procedure.

Crystallization and Structure Determination. Crystals were grown using the hanging drop vapor diffusion method. First, 10 μL protein solution [10 mg/mL protein in 50 mM Tris-HCl at pH 7.5, 50 mM NaCl, 1 mM DTT, 10 mM GSH, and 1 mM ethylenediaminetetraacetic acid (EDTA)] was mixed with 1 μL of 100 mM inhibitor DMSO solution. Then, equal amounts of this solution and precipitant solution (30% PEG 6000, 1% dioxane, 5 mM DTT, 5 mM GSH, and 50 mM Tris-HCl at pH 8.4 or 30% PEG 6000, 5 mM TCEP, 5 mM GSH, 1% dioxane, 5 mM $MgCl_2$, and 50 mM Tris-HCl at pH 8.4) were mixed and equilibrated over 1 mL precipitant solution. Rod-like crystals formed in about 1 week at room temperature and were optimized using seeding protocols. X-ray diffraction data were collected at the European Syncrotron Radiation Facility (ESRF), Grenoble, France, using an ADSC detector. Data were integrated and processed using MOSFLM and SCALA of the CCP4 suite.[44] The crystals belong to the space group $I4_1$ ($a = b = 123$ Å, and $c = 106$ Å) with two dimers in the asymmetric unit. The structures were solved by molecular replacement using Protein Data Bank (PDB) entry 1pd2 as the search model. The phases were refined using the CCP4 suite[44] and manual rebuilding using O.[45]

Trp-Fluorescent Measurements. The conditions used were 0.5 μM protein, Tris at pH 7.5, and 1 mM $MgCl_2$. Excitation wavelength was 284 nm, and emission wavelength was 336 nm. Controls were performed for a selected set of compounds by titration of a 1 μM L-tryptophan solution to determine the effect of absorption by the compound at 336 nm. Affinities were determined from a three parameter nonlinear least-squares fit of the function $F(x)$ to the experimental data

$$F(x) = F_{start} - (F_{start} - F_{end})PL/P$$

where F is the observed fluorescence. PL is the concentration of the protein–ligand complex, and P is the total protein concentration. The protein concentration limits the precision of the K_D determi-

nation for high-affinity binders. However, the tight binders were retested using different conditions, and the lower limit of the assay is estimated to be around 10 nM.

Library Design and Docking. A focused library for fragment screening was designed applying 1D filters (molecular weight < 200, and *c* log $P \leq 2$) to the in-house compound collection, obtaining 20 670 compounds. The starting format of the database was in SMILES, and Leatherface[46] (an in-house molecular editor based on the Daylight toolkit[47]) was used for generating protonation and tautomeric states; 3D coordinates were generated using CORINA[48] with explicit enumeration of stereocenters.

The compounds were then docked in the PGDS binding site using GOLD[49] with the standard mode settings and default parameters. The ligands were scored with GoldScore, and 10 poses per ligand were saved. The docking was carried out in the presence of glutathione. No water molecules were included in the binding site at this stage. After docking, a postfiltering method was applied that removed all of the molecules not forming a hydrogen-bond interaction with either Arg14 or Tyr152 (on the basis of the published PGD_2 binding mode[50]). The remaining poses were rescored with an in-house consensus scoring method, and 450 compounds were selected for NMR screening.

The same docking protocol was used for a virtual screening exercise, in which 5000 molecules (including molecules with $M_w > 200$) from the in-house compound collection were docked into the PGDS binding site. After postfiltering and rescoring as described above, the top 500 poses were manually inspected, which resulted in the selection of 30 compounds for testing; one of them showed micromolar potency (compound **4** in Figure 6e).

After the NMR hits were identified and complexes crystallized, further dockings were carried out to support the expansion rounds, and in all cases, the binding site of PGDS included the conserved water molecule identified by X-ray crystallography. The docking protocol was the same adopted for the library design, with postfiltering based on the identified pharmacophoric interactions.

Acknowledgment. We thank Igor Shamovski, David Laurent, Niek Dekker, and Henric Olsson for discussions and Josefine Cederfur and Richard Ernill for experimental contributions.

References

(1) Deprez-Poulain, R.; Deprez, B. Facts, figures and trends in lead generation. *Curr. Top. Med. Chem.* **2004**, *4*, 569–580.
(2) Bohacek, R. S.; McMartin, C.; Guida, W. C. The art and practice of structure-based drug design: A molecular modeling perspective. *Med. Res. Rev.* **1996**, *16*, 3–50.
(3) Teague, S. J.; Davis, A. M.; Leeson, P. D.; Oprea, T. The design of leadlike combinatorial libraries. *Angew. Chem., Int. Ed.* **1999**, *38*, 3743–3748.
(4) Wenlock, M. C.; Austin, R. P.; Barton, P.; Davis, A. M.; Leeson, P. D. A comparison of physiochemical property profiles of development and marketed oral drugs. *J. Med. Chem.* **2003**, *46*, 1250–1256.
(5) Lipinski, C. A. Lead- and drug-like compounds: The rule-of-five revolution. *Drug Discovery Today* **2004**, *1*, 341.
(6) Shuker, S. B.; Hajduk, P. J.; Meadows, R. P.; Fesik, S. W. Discovering high-affinity ligands for proteins: SAR by NMR. *Science* **1996**, *274*, 1531–1534.
(7) Fejzo, J.; Lepre, C. A.; Peng, J. W.; Bemis, G. W.; Ajay Murcko, M. A.; Moore, J. M. The SHAPES strategy: An NMR-based approach for lead generation in drug discovery. *Chem. Biol.* **1999**, *6*, 755–769.
(8) Böhm, H.-J.; Boehringer, M.; Bur, D.; Gmuender, H.; Huber, W.; Klaus, W.; Kostrewa, D.; Kuehne, H.; Luebbers, T.; Meunier-Keller, N.; Mueller, F. Novel inhibitors of DNA gyrase: 3D structure based biased needle screening, hit validation by biophysical methods, and 3D guided optimization. A promising alternative to random screening. *J. Med. Chem.* **2000**, *43*, 2664–2674.
(9) Maly, D. J.; Choong, I. C.; Ellman, J. A. Combinatorial target-guided ligand assembly: Identification of potent subtype-selective c-Src inhibitors. *Proc. Natl. Acad. Sci. U.S.A.* **2000**, *97*, 2419–2424.
(10) Leach, A. R.; Hann, M. M.; Burrows, J. N.; Griffen, E. Fragment screening: An introduction. In *Structure-Based Drug Discovery*; Hubbard, R. E., Ed.; Royal Society of Chemistry: Cambridge, U.K., 2006; pp 142–172.
(11) Hajduk, P. J.; Greer, J. A decade of fragment-based drug design: Strategic advances and lesson learned. *Nat. Rev. Drug Discovery* **2007**, *6*, 211–219.
(12) Carr, R.; Jhoti, H. Structure-based screening of low affinity compounds. *Drug Discovery Today* **2002**, *7*, 522–527.
(13) Lepre, C. A.; Moore, J. M.; Peng, J. W. Theory and applications of NMR-based screening in pharmaceutical research. *Chem. Rev.* **2004**, *104*, 3641–3675.
(14) Swayze, E. E.; Jefferson, E. A.; Sannes-Lowery, K. A.; Blyn, L. B.; Risen, L. M.; Arakawa, S.; Osgood, S. A.; Hofstadler, S. A.; Griffey, R. H. SAR by MS: A ligand based technique for drug lead discovery against structured RNA targets. *J. Med. Chem.* **2002**, *45*, 3816–3819.
(15) Card, G. L.; Blasdel, L.; England, B. P.; Zhang, C.; Suzuki, Y.; Gillette, S.; Fong, D.; Ibrahim, P. N.; Artis, D. R.; Bollag, G.; Milburn, M. V.; Kim, S.-H.; Schlessinger, J.; Zhang, K. Y. J. A family of phosphodiesterase inhibitors discovered by cocrystallography and scaffold-based drug design. *Nat. Biotechnol.* **2005**, *23*, 201–207.
(16) Hann, M. M.; Leach, A. R.; Harper, G. Molecular complexity and its impact on the probability of finding leads for drug discovery. *J. Chem. Inf. Model.* **2001**, *41*, 856–864.
(17) Hopkins, A. L.; Groom, C. R.; Alex, A. Ligand efficiency: A useful metric for lead selection. *Drug Discovery Today* **2004**, *9*, 431.
(18) Rees, D. C.; Congreve, M.; Murray, C. W.; Carr, R. Fragment-based lead discovery. *Nat. Rev. Drug Discovery* **2004**, *3*, 660–672.
(19) Hayaishi, O.; Urade, Y. Prostaglandin D2 in sleep-wake regulation: Recent progress and perspectives. *Neuroscientist* **2002**, *8*, 12–15.
(20) Whittle, B. J.; Hamid, S.; Lidbury, P.; Rosam, A. C. Specificity between the anti-aggregatory actions of prostacyclin, prostaglandin E1 and D2 on platelets. *Adv. Exp. Med. Biol.* **1985**, *192*, 109–125.
(21) Hirai, H.; Tanaka, K.; Yoshie, O.; Ogawa, K.; Kenmotsu, K.; Takamori, Y.; Ichimasa, M.; Sugamura, K.; Nakamura, M.; Takano, S.; Nagata, K. Prostaglandin D2 selectively induces chemotaxis in T helper type 2 cells, eosinophils, and basophils via seven-transmembrane receptor CRTH2. *J. Exp. Med.* **2001**, *193*, 255–262.
(22) Hardy, C.; Robinson, C.; Tattersfield, A.; Holgate, S. The bronchoconstrictor effect of inhaled prostaglandin D2 in normal and asthmatic men. *N. Engl. J. Med.* **1984**, *311*, 209–213.
(23) Urade, Y.; Fujimoto, N.; Ujihara, M.; Hayaishi, O. Biochemical and immunological characterization of rat spleen prostaglandin D synthetase. *J. Biol. Chem.* **1987**, *262*, 3820–3825.
(24) Urade, Y.; Hayaishi, O. Biochemical, structural, genetic, physiological, and pathophysiological features of lipocalin-type prostaglandin D synthase. *Biochim. Biophys. Acta* **2000**, *1482*, 271.
(25) Urade, Y.; Hayaishi, O. Prostaglandin D synthase: Structure and function. *Vitam. Horm.* **2000**, *58*, 89–120.
(26) Kanaoka, Y.; Ago, H.; Inagaki, E.; Nanayama, T.; Miyano, M.; Kikuno, R.; Fujii, Y.; Eguchi, N.; Toh, H.; Urade, Y.; Hayaishi, O. Cloning and crystal structure of hematopoietic prostaglandin D synthase. *Cell* **1997**, *90*, 1095.
(27) Inoue, T.; Irikura, D.; Okazaki, N.; Kinugasa, S.; Matsumura, H.; Uodome, N.; Yamamoto, M.; Kumasaka, T.; Miyano, M.; Kai, Y.; Urade, Y. Mechanism of metal activation of human hematopoietic prostaglandin D synthase. *Nat. Struct. Mol. Biol.* **2003**, *10*, 296.
(28) Matsuoka, T.; Hirata, M.; Tanaka, H.; Takahashi, Y.; Murata, T.; Kabashima, K.; Sugimoto, Y.; Kobayashi, T.; Ushikubi, F.; Aze, Y.; Eguchi, N.; Urade, Y.; Yoshida, N.; Kimura, K.; Mizoguchi, A.; Honda, Y.; Nagai, H.; Narumiya, S. Prostaglandin D2 as a mediator of allergic asthma. *Science* **2000**, *287*, 2013–2017.
(29) Oguma, T.; Palmer, L. J.; Birben, E.; Sonna, L. A.; Asano, K.; Lilly, C. M. Role of prostanoid DP receptor variants in susceptibility to asthma. *N. Engl. J. Med.* **2004**, *351*, 1752–1763.
(30) Shichijo, M.; Sugimoto, H.; Nagao, K.; Inbe, H.; Encinas, J. A.; Takeshita, K.; Bacon, K. B.; Gantner, F. Chemoattractant receptor-homologous molecule expressed on Th2 cells activation in vivo increases blood leukocyte counts and its blockade abrogates 13,14-dihydro-15-keto-prostaglandin D2-induced eosinophilia in rats. *J. Pharmacol. Exp. Ther.* **2003**, *307*, 518–525.
(31) Uller, L.; Mathiesen, J.; Alenmyr, L.; Korsgren, M.; Ulven, T.; Hogberg, T.; Andersson, G.; Persson, C.; Kostenis, E. Antagonism of the prostaglandin D2 receptor CRTH2 attenuates asthma pathology in mouse eosinophilic airway inflammation. *Respir. Res.* **2007**, *8*, 16.
(32) Li, L.; Yang, Y.; Stevens, R. L. RasGRP4 regulates the expression of prostaglandin D2 in human and rat mast cell lines. *J. Biol. Chem.* **2003**, *278*, 4725–4729.
(33) Holgate, S.; Burns, G.; Robinson, C.; Church, M. Anaphylactic- and calcium-dependent generation of prostaglandin D2 (PGD2), thromboxane B2, and other cyclooxygenase products of arachidonic acid by dispersed human lung cells and relationship to histamine release. *J. Immunol.* **1984**, *133*, 2138–2144.
(34) Lewis, R.; Soter, N.; Diamond, P.; Austen, K.; Oates, J.; Roberts, L. 2D Prostaglandin D2 generation after activation of rat and human mast cells with anti-IgE. *J. Immunol.* **1982**, *129*, 1627–1631.

(35) Wenzel, S.; Westcott, J.; Smith, H.; Larsen, G. Spectrum of prostanoid release after bronchoalveolar allergen challenge in atopic asthmatics and in control groups. An alteration in the ratio of bronchoconstrictive to bronchoprotective mediators. *Am. Rev. Respir. Dis.* **1989**, *139*, 450–457.
(36) Ikai, K.; Ujihara, M.; Fujii, K.; Urade, Y. Inhibitory effect of tranilast on prostaglandin D synthase. *Biochem. Pharmacol.* **1989**, *38*, 2673–2676.
(37) Dalvit, C.; Pevarello, P.; Tatò, M.; Veronesi, M.; Vulpetti, A.; Sundström, M. Identification of compounds with binding affinity to proteins via magnetization transfer from bulk water. *J. Biomol. NMR* **2000**, *18*, 65–68.
(38) Hesterkamp, T.; Barker, J.; Davenport, A.; Whittaker, M. Fragment based drug discovery using fluorescence correlation spectroscopy techniques: Challenges and solutions. *Curr. Top. Med. Chem.* **2007**, *7*, 1582–1591.
(39) Hopkins, A. L.; Groom, C. R.; Alex, A. Ligand efficiency: A useful metric for lead selection. *Drug Discovery Today* **2004**, *9*, 430–431.
(40) Kirshenbaum, A. S.; Akin, C.; Wu, Y.; Rottem, M.; Goff, J. P.; Beaven, M. A.; Rao, V. K.; Metcalfe, D. D. Characterization of novel stem cell factor responsive human mast cell lines LAD 1 and 2 established from a patient with mast cell sarcoma/leukemia; activation following aggregation of FcϵRI or FcγRI. *Leuk. Res.* **2003**, *27*, 677–682.
(41) Pervushin, K.; Riek, R.; Wider, G.; Wutrich, K. Attenuated T-2 relaxation by mutual cancellation of dipole−dipole coupling and chemical shift anisotropy indicates an avenue to NMR structures of very large biological macromolecules in solution. *Proc. Natl. Acad. Sci. U.S.A.* **1997**, *94*, 12366–12371.
(42) Delaglio, F.; Grzesiek, S.; Vuister, G. W.; Zhu, G.; Pfeifer, J.; Bax, A. NMRPipe: A multidimensional spectral processing system based on UNIX pipes. *J. Biomol. NMR* **1995**, *6*, 277–293.
(43) Johnson, B. A.; Blevins, R. A. NMR View: A computer program for the visualization and analysis of NMR data. *J. Biomol. NMR* **1994**, *4*, 603–614.
(44) Collaborative Computational Project, Number 4. The CCP4 suite: Programs for protein crystallography. *Acta Crystallogr., Sect. D: Biol. Crystallogr.* **1994**, *50*, 760−763.
(45) Jones, T. A.; Zou, J. Y.; Cowan, S. W.; Kjeldegaard, M. Improved methods for building protein models in electron density maps and the location of errors in these models. *Acta Crystallogr., Sect. A: Found. Crystallogr.* **1991**, *47*, 110–119.
(46) Kenny, P. W.; Sadowski, J. Structure modification in chemical databases. In *Chemoinformatics in Drug Discovery*; Oprea, T. I., Ed.; Wiley-VCH: Weinheim, Germany, 2004; pp 271–285.
(47) Daylight Chemical Information Systems, Inc., http://www.daylight.com.
(48) Gasteiger, J.; Rudolf, C.; Sadowski, J. Automatic Generation of 3D atomic coordinates for organic molecules. *Tetrahedron Comput. Methodol.* **1990**, *3*, 537–547.
(49) Jones, G.; Willett, P.; Glen, R. C.; Leach, A. R.; Taylor, R. Development and validation of a genetic algorithm for flexible docking. *J. Mol. Biol.* **1997**, *267*, 727–748.
(50) Kanaoka, Y.; Ago, H.; Inagaki, E.; Nanayama, T.; Miyano, M.; Kikuno, R.; Fujii, Y.; Eguchi, N.; Toh, H.; Urade, Y.; Hayaishi, O. Cloning and crystal structure of hematopoietic prostaglandin D synthase. *Cell* **1999**, *96*, 449.

JM701509K